PHYSICAL REVIEW D **79,** 094505 (2009)

Extracting electric polarizabilities from lattice QCD

W. Detmold,[1,2,*] B. C. Tiburzi,[3,†] and A. Walker-Loud[1,‡]

[1]*Department of Physics, College of William and Mary, Williamsburg, Virginia 23187-8795, USA*
[2]*Thomas Jefferson National Accelerator Facility, Newport News, Virginia 23606, USA*
[3]*Maryland Center for Fundamental Physics, Department of Physics, University of Maryland, College Park, Maryland 20742-4111, USA*

(Received 16 April 2009; published 15 May 2009)

Charged and neutral, pion and kaon electric polarizabilities are extracted from lattice QCD using an ensemble of anisotropic gauge configurations with dynamical clover fermions. We utilize classical background fields to access the polarizabilities from two-point correlation functions. Uniform background fields are achieved by quantizing the electric field strength with the proper treatment of boundary flux. These external fields, however, are implemented only in the valence quark sector. A novel method to extract charge particle polarizabilities is successfully demonstrated for the first time.

DOI: 10.1103/PhysRevD.79.094505 PACS numbers: 12.38.Gc

I. INTRODUCTION

A staple component of electrodynamics courses is the electric polarizability. Neutral materials immersed in electric fields polarize. At the atomic scale, electron clouds distort creating microscopic dipole moments that orient opposite the applied field to minimize the energy. This simple principle accounts for dielectric properties of materials, a range of intermolecular forces, and properties of atoms and nuclei in applied fields. At the femtoscale, hadrons too polarize in applied fields, but only against the strong chromodynamic interactions confining their electrically charged quarks into hadrons.

Understanding properties of hadrons quantitatively is formidable. Quark and gluon interactions must be treated nonperturbatively for which lattice QCD has been developed; see [1] for a review. Low-energy properties of hadrons, however, can be described using an effective theory of QCD, based upon treating pseudoscalar mesons as the Goldstone modes arising from spontaneous chiral symmetry breaking. A picture of hadrons emerges from chiral dynamics: that of a hadronic core surrounded by a pseudoscalar meson cloud. As some pseudoscalar mesons are charged, polarizabilities of hadrons encode the stiffness of the charged meson cloud (as well as that of the core). The form of pseudoscalar meson polarizabilities is consequently strongly constrained by chiral dynamics [2–4]. Beyond the leading order, however, results depend on essentially unknown low-energy constants, which currently must be estimated in a model-dependent fashion. For the case of the charged pion, confrontation of these results with experiment has proven difficult, e.g. from the original measurement [5], to the most recent [6], extracted results disagree with predictions made using chiral dynamics. New results with higher statistics and the first kaon results are anticipated from COMPASS at CERN [7].

Lattice gauge theory simulations provide a first principles approach to determine hadronic polarizabilities from QCD, crucially test predictions from chiral dynamics, and confront experiment. Indeed the unknown low-energy constants of chiral perturbation theory can be determined by matching to lattice QCD computations. Furthermore, the ability to vary the quark mass allows one to directly explore the chiral behavior of observables, investigate the convergence properties of the perturbative expansion, and thereby test the predictions of the effective theory. The highly constrained form for hadronic polarizabilities within chiral perturbation theory leads to a stringent test of low-energy QCD dynamics.

Electric polarizabilities of neutral hadrons have been calculated with lattice QCD using the quenched approximation at pion masses greater than 500 MeV [8,9]. There has also been a fully dynamical calculation of the neutron electric polarizability at a pion mass of 760 MeV [10]. These calculations do not employ constant electric fields but attempt to mitigate effects from field gradients by imposing Dirichlet boundary conditions on the quark fields in the time and/or space directions. Such an approach leads to uncertainties that are difficult to quantify. In this work, we report on calculations of pseudoscalar meson polarizabilities using lattice QCD with dynamical configurations. A salient feature of our computation is that it utilizes a periodic lattice action with everywhere constant electric fields. Our calculations of meson polarizabilities are the first such to include effects from dynamical quarks. At this stage, however, we are restricted to electrically neutral sea quarks. Correcting for this malady would re-

*wdetmold@wm.edu
†bctiburz@umd.edu
‡walkloud@wm.edu

quire at least an order of magnitude greater computing power.[1] Furthermore, we demonstrate for the first time how to extract charge particle polarizabilities from lattice two-point correlation functions.

We begin in Sec. II by describing the implementation of constant external fields on a lattice. The appendix considers the effect of nonuniform fields. Next in Sec. III, we detail how lattice two-point correlation functions can be utilized to extract the electric polarizabilities of both charged and neutral particles. Details of our lattice study are then presented in Sec. IV, and summarized in a conclusion, Sec. V.

II. CONSTANT FIELDS ON A LATTICE

To produce a constant electric field, $\vec{\mathcal{E}} = \mathcal{E}\hat{z}$, we use the Euclidean space vector potential,

$$A_\mu(x) = (0, 0, -\mathcal{E}x_4, 0), \tag{1}$$

where $\mathcal{E}$ is a real-valued parameter. The analytic continuation $\mathcal{E} \to -i\mathcal{E}_{\rm M}$ produces a real-valued electric field in Minkowski space. Generally this continuation cannot be performed using numerical data because of nonperturbative effects, e.g. the Schwinger pair-creation mechanism [13] is absent in Euclidean space. We are interested, however, solely in quantities that are perturbative in the external field strength, for which the naïve continuation produces the correct Minkowski space physics; see [14] for explicit details.

To implement the background field on the lattice, we modify the $SU(3)$ color gauge links, $U_\mu(x)$, for each quark flavor by multiplying by the color-singlet Abelian links, $U_\mu^{(\mathcal{E})}(x)$, for the external field, namely,

$$U_\mu(x) \to U_\mu(x)U_\mu^{(\mathcal{E})}(x), \tag{2}$$

where $U_\mu^{(\mathcal{E})}(x) = \exp[iQA_\mu(x)]$, Q is the quark electric charge, and $A_\mu(x)$ is given in Eq. (1). As this multiplication is carried out on preexisting gauge configurations, the sea quarks remain electrically neutral. This approximation is imposed because of computational restrictions which will not be rectified in the near future without a significant increase in resources.

The inclusion of the field via Eq. (2) does not lead to a constant electric field. On a torus, constant gauge fields require quantization [15–17]. The basic argument is as follows. With periodic boundary conditions,[2] the action is defined on a torus, which is a closed surface. For the field we wish to implement, the only plane with nonvanishing flux is the x_3-x_4 plane. The total area of the x_3-x_4 plane is βL, where L is the length of the x_3 direction, and β is the length of the x_4 direction. Because the torus is a closed surface, however, there can be no net flux through the x_3-x_4 plane (modulo 2π), i.e. $\Phi = Q\mathcal{E}\beta L \equiv 2\pi n$, with n as an integer. This leads to the 't Hooft quantization condition

$$\mathcal{E} = \frac{2\pi n}{q_d \beta L}. \tag{3}$$

Here we have used the down quark electric charge, $q_d = -1/3e$, and note that the up quark will necessarily encounter properly quantized fields when Eq. (3) is met because $q_u = -2q_d$.

The argument presented for constant gauge fields applies to a continuous torus, and must be modified for a discrete torus; see e.g. [18–20]. On a discrete torus, each of the elementary plaquettes must be identical with value: $\exp(iQ\mathcal{E})$ to arrive at the constant electric field $\mathcal{E}$. With Eq. (2), the plaquettes are identical in the bulk of the lattice but not at the boundary, where there are L plaquettes with differing flux. Each of these plaquettes wraps around from $x_4 = \beta - 1$ to $x_4 = 0$, with the common value $\exp[iQ\mathcal{E}(1-\beta)]$. This unwanted flux can be eliminated on $L-1$ of the plaquettes by including additional transverse links, $U_\mu^{(\mathcal{E})_\perp}(x)$, at the boundary,

$$U_\mu(x) \to U_\mu(x)U_\mu^{(\mathcal{E})}(x)U_\mu^{(\mathcal{E})_\perp}(x), \tag{4}$$

with $U_\mu^{(\mathcal{E})_\perp}(x) = \exp[iQ\mathcal{E}\beta x_3 \delta_{\mu 4}\delta_{x_4,\beta-1}]$. Now the field through every plaquette is $\mathcal{E}$, with only one exception: the plaquette at the far corner of the lattice, $(x_3, x_4) = (L-1, \beta-1)$ that wraps around to $x_3 = 0$ and $x_4 = 0$. The value of this plaquette is $\exp[iQ\mathcal{E}(1-\beta L)]$, which is identical to the plaquette in the bulk of the lattice provided 't Hooft's quantization condition, Eq. (3), is met. We have previously demonstrated the effects of using nonquantized field values, finding non-negligible shifts in particle spectra [21]. We summarize our findings in the appendix. In this work, we implement the external field using Eq. (4), and quantized values for the field strength $\mathcal{E}$ in Eq. (3). This choice corresponds to a completely periodic lattice gauge action, and thus corresponds to a field theory at a finite (but low) temperature in the continuum limit.

[1] Pseudoscalar meson polarizabilities first depend on sea quark charges at next-to-next-to-leading order in the chiral expansion [11,12]. It is thus possible to extract physical information from simulations with vanishing sea quark charges by utilizing chiral perturbation theory. As the current study is restricted to one volume and one pion mass, we leave this investigation to future work.

[2] The argument applies equally well to the case of twisted boundary conditions on the matter fields $\psi(x)$ of the form $\psi(x + L\hat{x}_j) = e^{i\theta_j}\psi(x)$, and analogously for the time direction. Dirichlet boundary conditions, on the other hand, inevitably lead to problems.

III. CORRELATION FUNCTIONS

For a neutral particle, it is straightforward to calculate the electric polarizability using standard lattice spectroscopy [8].[3] One merely matches the long-time behavior of Euclidean two-point functions, $g(x_4, \mathcal{E})$, computed in QCD to the expectations of the effective hadronic theory to deduce the particle's energy. The lattice two-point function has the form

$$g(x_4, \mathcal{E}) = \sum_{\boldsymbol{x}} \langle 0|\phi(x)\phi^\dagger(0)|0\rangle_{\mathcal{E}}, \tag{5}$$

where ϕ is an interpolating field for the particle of interest (e.g. $\phi = \bar{d}\gamma_5 s$ for the K^0), and the subscript $\mathcal{E}$ denotes that the correlation function is determined in the background electric field. This correlation function is matched onto the correlator $G(x_4, \mathcal{E})$, in the hadronic theory,

$$G(x_4, \mathcal{E}) = Z(\mathcal{E})e^{-E(\mathcal{E})x_4} + Z'(\mathcal{E})e^{-E'(\mathcal{E})x_4} + \ldots, \tag{6}$$

where the ellipsis represents exponentially suppressed contributions beyond the first excited state. The ground-state particle's energy, $E(\mathcal{E})$, has a series expansion in the external field strength

$$E(\mathcal{E}) = M + \frac{1}{2}4\pi\alpha_E\mathcal{E}^2 - \frac{1}{4!}(4\pi)^2\bar{\alpha}_{EEE}\mathcal{E}^4 + \ldots, \tag{7}$$

where M is the particle's mass, α_E its electric polarizability, and $\bar{\alpha}_{EEE}$ is a multiple electric dipole interaction strength. Here the ellipsis represents terms at higher order in the strength of the field. The sign of the polarizability term (quadratic Stark shift) is positive due to our treatment in Euclidean space. The amplitudes, $Z(\mathcal{E})$ and $Z'(\mathcal{E})$, also have expansions in even powers of $\mathcal{E}$. As explained below, we are forced in our particular computations to consider contributions from excited states, shown in Eq. (6). The energy, E', of the first excited state has an analogous weak field expansion in terms of the mass M', polarizability α'_E, etc..

When charged particles are subjected to constant electric fields, we again match the lattice correlation function, $g(x_4, \mathcal{E})$, to the correlator calculated in the hadronic theory. With sufficiently weak fields, quarks and gluons will still hadronize into a tower of states of the same quantum numbers, specifically of the same charge. For times, x_4, long compared to that set by the excited state mass, $x_4 \gg \tau' \sim 1/M'$, the excited state contributions to the two-point function will still be exponentially suppressed (albeit not a simple exponential). For times beyond τ', we can assume the two-point correlation function will be dominated by the ground state. As this state is charged, the behavior of the correlation function will have a more complicated form than a simple exponential falloff with time.

For a relativistic scalar particle of charge Q, consider the single-particle effective action in the hadronic theory. As the particle is composite, there are both Born and non-Born terms in the action. The non-Born terms account for non-minimal couplings of the field to the particle, such as polarizabilities. These couplings can be summed, as in the case of a neutral particle, into the energy, $E(\mathcal{E})$, defined above. The Born couplings additionally must be summed to arrive at the charged particle two-point function. For the field specified by Eq. (1), the equations of motion for a scalar particle are exactly solvable, and lead to the two-point function in the hadronic theory

$$G(x_4, \mathcal{E}) = Z(\mathcal{E})D(x_4, E(\mathcal{E}), \mathcal{E}) + Z'(\mathcal{E})D(x_4, E'(\mathcal{E}), \mathcal{E}) + \ldots, \tag{8}$$

with the ellipsis representing contributions beyond the first excited state, and the relativistic propagator of a charged scalar, $D(x_4, E(\mathcal{E}), \mathcal{E})$, given by [14]

$$D(x_4, E(\mathcal{E}), \mathcal{E}) = \int_0^\infty ds \sqrt{\frac{Q\mathcal{E}}{2\pi \sinh(Q\mathcal{E}s)}} \times \exp\left[-\frac{Q\mathcal{E}x_4^2}{2}\coth(Q\mathcal{E}s) - \frac{E(\mathcal{E})^2 s}{2}\right], \tag{9}$$

where $E(\mathcal{E})$ can no longer be interpreted as the energy but remains given by Eq. (7). Classically $E(\mathcal{E})$ is the rest energy of the charged particle. The analogy to a classically accelerating particle occurs at the level of the particle's action. Interpreting the Euclidean time behavior of the particle's motion on a compact space in terms of acceleration proves difficult. For $Q = 0$, this propagator properly reduces to Eq. (6). For sufficiently weak fields, or equivalently short times, the $\mathcal{O}(\mathcal{E}^2)$ term in the series expansion of the correlator reproduces the nonrelativistic result derived in [24]. Because of our particular anisotropic lattices, we include contributions to the two-point function from the first excited state thereby stabilizing the extraction of ground-state parameters. The quantum numbers of the excited state are identical to the ground state, i.e. $Q' = Q$.

[3] Strictly speaking this is only true at infinite volume. At finite volume, there are additional effects stemming from boundary conditions and the compact nature of the external gauge field [22,23]. As we employ only one lattice volume to demonstrate our methods, we neglect these additional corrections at this stage. Further analysis with multiple volumes and multiple pion masses is needed to control these systematics.

IV. LATTICE RESULTS

To demonstrate our method for extracting meson polarizabilities from lattice two-point functions, we have employed an ensemble of anisotropic gauge configurations with $2+1$ flavors of dynamical clover fermions [25,26]. The ensemble we use consists of 200 lattices of size $20^3 \times 128$. After an initial 1000 thermalization trajectories, the lattices were chosen from an ensemble of 7000 spaced either by 20 or 40 to minimize autocorrelations. The spatial lattice spacing of these configurations is $a_s = 0.123$ fm [25,26], with a nonperturbatively tuned anisotropy parameter of $\xi \equiv a_s/a_t = 3.5$, where a_t is the temporal lattice spacing. The finer temporal spacing affords us the ability to better fit nonstandard behavior for two-point correlation functions, and is critical for this analysis. On the ensemble, the renormalized strange mass is near the physical value, while the renormalized light quark mass leads to a pion mass of $m_\pi \approx 390$ MeV.

On each configuration, we compute at least 10 up quark propagators, 10 down quark propagators, and 10 strange quark propagators with random spatial source locations. Multiple inversions were made efficient using the EigCG inverter [27]. Interpolating fields at the source are generated from gauge covariantly Gaussian-smeared quark fields [28,29] on a stout-smeared [30] gauge field in order to optimize the overlap onto the ground state. Interpolating fields at the sink are constructed from local quark fields. Each propagator is located with source time at $\tau_{\rm src} = 0$. Randomization of the source time location, while improving the statistical sampling, would complicate the extraction of both charged and neutral meson correlation functions, as two-point functions are no longer time translationally invariant. For charged particles, the correlator in Eq. (8) is explicitly a function of the sink time slice and not simply a function of the source-sink separation (the full dependence on source time is given in [14]), while for neutral particles the violation of time-translation invariance arises from volume effects.

The external field was implemented using Eq. (4), and propagators were computed for nine values of the field strength, n, corresponding to the integer appearing in the quantization condition, Eq. (3). We use $n = 0$, which corresponds to a vanishing external field, as well as $n = \pm 1, \ldots, \pm 4$. On our lattices, the expansion parameter governing the deformation of a hadron's pion cloud is given by [14]

$$\left(\frac{e\mathcal{E}}{m_\pi^2}\right)^2 = 0.18 n^2. \tag{10}$$

From the size of this parameter, we anticipate the need to include terms beyond quadratic order in the electric-field expansion of hadron energies. In our analysis, we include terms up to quartic order. Larger lattices will be required for better control over systematics relating to the electric-field expansion of observables.

Meson two-point functions were obtained for each source location on a given configuration. Individual results for the multiple source locations on each configuration were then source averaged. This procedure was carried out for each value of the external field. To satisfy invariance under parity transformations, under which $\mathcal{E} \to -\mathcal{E}$, we took the geometric mean of correlators calculated at n, and $-n$ on each configuration. This reduced the set of fields to five magnitudes corresponding to the integers, $n = 0, \ldots, 4$. The ensemble of correlation functions was then used to generate 200 bootstrap ensembles. Fits to the bootstrapped ensemble were performed as described below.[4]

A. Neutral pion and kaon

Bootstrapped correlators for the neutral pion and kaon were obtained using the procedure described above. As we use standard spectroscopy to determine the polarizabilities for neutral particles, we handle these mesons first. To facilitate the discussion, we consider the standard effective mass, given by

$$M_{\rm eff}(t) = -\log\frac{g(t+1,\mathcal{E})}{g(t,\mathcal{E})}, \tag{11}$$

where $g(t,\mathcal{E})$ is the bootstrap ensemble-averaged correlator. Error bars on the effective mass are determined using the bootstrap ensemble. Effective-mass plots for the neutral pion and neutral kaon are shown in Fig. 1. For the neutral pion, so far we have only calculated the connected part of the correlation function. The effective-mass plot should exhibit a plateau over a range of time when the ground state saturates the correlation function. The temporal extent of our anisotropic lattices is $\beta = 128$ $a_t = 4.5$ fm, which is considerably smaller than typical isotropic lattices, where $\beta > 7.5$ fm. As one must wait long enough for the excited states to drop out, the pion and kaon effective masses never plateau (or barely exhibit a plateau) because of the backward propagating image from the time boundary.

To extract the ground-state properties, we fit the correlation function $g(t,\mathcal{E})$ using the two-state form of $G(t,\mathcal{E})$ in Eq. (6) augmented to include a backwards propagating ground state, and backwards propagating excited state (i.e. a sum of two hyperbolic cosines). We use a correlated chi-squared analysis to fit the time dependence of the bootstrap ensemble of correlators. To determine the fit window, we use black box methods comparing single and

[4]We have performed multiple differing procedures to analyze the data, of which only one is described in detail in the text. Throughout we will comment on the alternate procedures. Most notably, fits have been performed using a jackknife procedure to determine uncertainties, and with a separate analysis of the positive and negative values of the field strength. Effects of correlations in the data have been investigated by blocking neighboring configurations, and consistent results have been obtained.

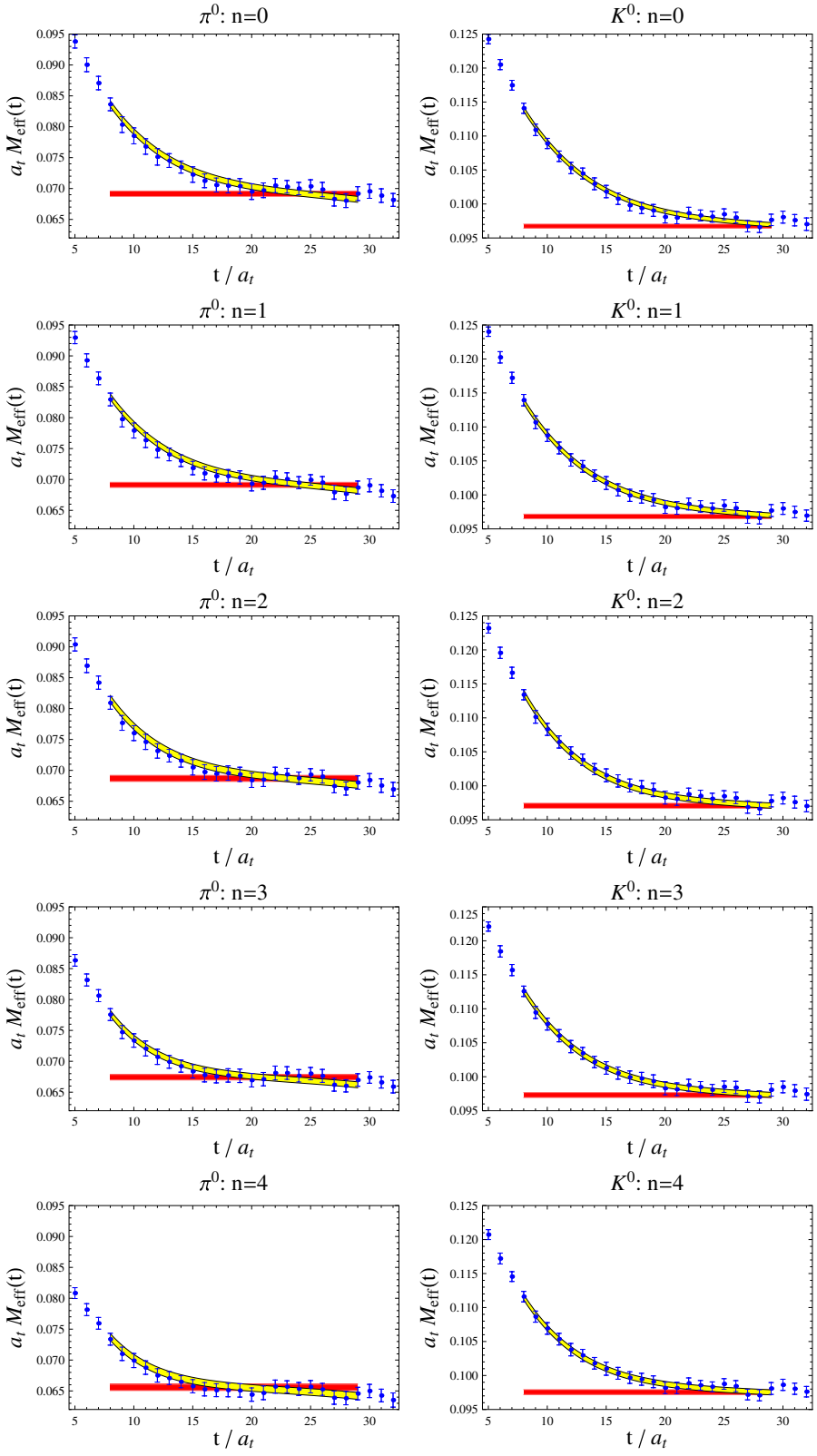

FIG. 1 (color online). Effective-mass plots for the (connected) neutral pion and neutral kaon. Values for n correspond to the magnitude of the quantized electric field $\mathcal{E}$, Eq. (3). Curved bands show fits to the correlation functions. For each plot, the band spans the fit window, and the width is set by the uncertainty in the ground-state energy. The flat bands shown are ground-state energies with uncertainty for each field value. On a lattice of infinite time extent, the effective masses should asymptote to these bands over long times.

TABLE I. Summary of fit results for neutral meson two-point functions for $8 \leq t \leq 29$. Here π^0 refers to the connected part of the correlation function, the fine-structure constant is $\alpha_{\text{f.s.}} = e^2/4\pi$, and $1 - P$ is the integrated chi-squared. All quoted values are averages over the bootstrap ensemble, and are given in dimensionless lattice units. For the electric polarizability, $\alpha_E^{\text{latt}} = \alpha_E(2\alpha_{\text{f.s.}} a_t a_s^2)^{-1}$ and the higher-order coupling, $\bar{\alpha}_{EEE}^{\text{latt}} = \bar{\alpha}_{EEE}(4!\alpha_{\text{f.s.}}^2 a_t^3 a_s^4)^{-1} 10^{-3}$. The first half of the table summarizes the time-correlated fits to the energies in each field, while the second half summarizes the field-correlated fits. The fits I and II are described in the text. The second uncertainty on the polarizabilities is an estimate of the systematic due to the choice of fit window as explained in the text.

π^0	n	$a_t E(\mathcal{E})$	$1 - P$	K^0	n	$a_t E(\mathcal{E})$	$1 - P$
	0	0.0692(5)	0.90		0	0.0967(3)	0.89
‘	1	0.0691(5)	0.70		1	0.0968(4)	0.87
	2	0.0687(5)	0.76		2	0.0971(4)	0.84
	3	0.0674(5)	0.74		3	0.0973(4)	0.92
	4	0.0656(5)	0.83		4	0.0976(4)	0.94

π^0	$a_t M$	α_E^{latt}	$\bar{\alpha}_{EEE}^{\text{latt}}$	$1 - P$	K^0	$a_t M$	α_E^{latt}	$\bar{\alpha}_{EEE}^{\text{latt}}$	$1 - P$
I	0.0692(1)	−2.6(5)(9)	1.8(5)	0.69	I	0.0968(1)	1.5(4)(7)	0.6(5)	0.97
II	0.0692(1)	−1.0(1.5)(1.4)	5.3(3.2)	0.92	II	0.0967(1)	1.8(1.0)(1.9)	1.3(1.9)	0.95

double effective masses; see [31–33] for details on the latter. We found the same fit window, $8 \leq t \leq 29$, could be used for a given particle for every value of the field strength. Alternate fits on the same window without backwards propagating states result in a 1.5% shift of the neutral pion energies, and a negligible shift of the kaon energies.

As the parameters $Z(\mathcal{E})$ and $Z'(\mathcal{E})$ enter the fit function $G(t, \mathcal{E})$ linearly, we utilize variable projection (see [31] for references) to reduce the number of fit parameters from four down to two, namely, just the energies $E(\mathcal{E})$ and $E'(\mathcal{E})$.[5] We perform these two-state fits on the entire bootstrap ensemble arriving at an ensemble of energies for each magnitude of the electric field $\mathcal{E}$, in particular $\{\boldsymbol{E}_i(\mathcal{E})\}$ for the ground state, where i indexes the bootstrap sample, $i = 1, \ldots, N$. As the ensembles of configurations for different field strengths are generated from the same underlying lattice configurations, correlations between the energies for different field strengths will be significant and it is important to account for these. On the bootstrap ensemble of energies, we perform electric-field correlated fits to the energy function $E(\mathcal{E})$ given in Eq. (7). With the ensemble average energies denoted by $\boldsymbol{E}(\mathcal{E}) = \frac{1}{N}\sum_i \boldsymbol{E}_i(\mathcal{E})$, we minimize the correlated chi-squared, namely,

$$\chi^2 = \sum_{\mathcal{E},\mathcal{E}'} [\boldsymbol{E}(\mathcal{E}) - E(\mathcal{E})] C^{-1}_{\mathcal{E},\mathcal{E}'} [\boldsymbol{E}(\mathcal{E}') - E(\mathcal{E}')], \tag{12}$$

with the field-strength correlation matrix, $C_{\mathcal{E},\mathcal{E}'}$, given by

$$C_{\mathcal{E},\mathcal{E}'} = \frac{1}{N-1} \sum_{i=1}^{N} [\boldsymbol{E}(\mathcal{E}) - \boldsymbol{E}_i(\mathcal{E})][\boldsymbol{E}(\mathcal{E}') - \boldsymbol{E}_i(\mathcal{E}')]. \tag{13}$$

Because all three fit parameters, M, α_E, and $\bar{\alpha}_{EEE}$, enter the fit function $E(\mathcal{E})$ linearly, the chi-squared minimization can be done analytically. Fits to the energy function are carried out on the bootstrap ensemble, resulting fit parameters are averaged, and the uncertainties from fitting and bootstrapping are added in quadrature. We perform two different field-correlated fits as follows: (I) a fit to all five field strengths using Eq. (7), (II) the same fit function but with the largest field strength excluded. Finally, to estimate the systematics due to the choice of fit window, we performed uncorrelated fits to the electric-field dependence of meson energies determined on adjacent fit windows. We chose the nine fit windows obtained by varying the start and end times by one unit in either direction. On each time window, we determined the electric polarizability. The systematic uncertainty on α_E due to the fit window is estimated as the standard deviation of the extracted α_E over the various adjacent windows. Fit details and extracted parameters are tabulated in Table I.

From the extracted polarizabilities, we can investigate the electric-field dependence of meson energies. This is done in Fig. 2 for the neutral pion and neutral kaon. For the connected part of the neutral pion, we see downward curvature of the energy with respect to increasing $\mathcal{E}$, while for the neutral kaon the energy is comparatively quite flat. In physical units, the polarizabilities $\alpha_E^{\pi^0}$, and $\alpha_E^{K^0}$, are not consistent with naïve expectations. To attempt a qualitative explanation for the size of the ground-state polarizabilities, we compare our results with predictions from chiral perturbation theory. The neutral pion electric polarizability at one-loop is negative [34,35]. While this is surprising, the

[5]We also analyze correlation functions by fitting the effective masses with two states. These three parameter fits give consistent results.

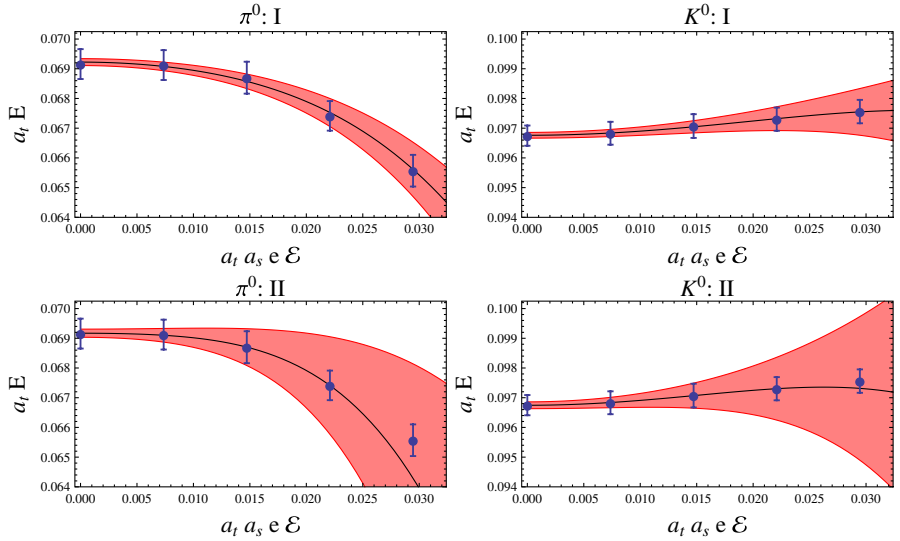

FIG. 2 (color online). Plots of correlated fits to the electric-field dependence of neutral meson energies. For each field strength, the bootstrap averaged energies are plotted with error bars reflecting the uncertainty from statistics and fitting. Fits I and II to the $\mathcal{E}$ dependence are also shown with the plotted bands reflecting the uncertainty in the parameters appearing in Eq. (7).

one-loop polarizability arises solely from the disconnected contraction between quark basis η_u and η_d mesons [11]. Hence the negative sign owes to group theory weight of η_u versus η_d in the pion interpolating field, $\pi^0 \sim \frac{1}{\sqrt{2}}(\eta_u - \eta_d)$. As we have only calculated the connected part of the correlator, chiral perturbation theory suggests that $\alpha_E^{\pi^0}$ is an order of magnitude smaller than the naïve expectation. While our result is of this magnitude, it is of the wrong sign (the average of η_u and η_d polarizabilities should be positive). This negative value could arise from volume effects, which are known to be nonvanishing at next-to-leading order in chiral perturbation theory [23]. For the neutral kaon polarizability, the one-loop chiral computation vanishes, even with electrically neutral sea quarks [12]. Our extracted neutral kaon polarizability, however, is smaller than typical two-loop contributions. Because the dominant volume corrections arise from pion loops, we expect the neutral pion and kaon volume effects to be of the same size. If the negative result for the connected π^0 is due to volume corrections, then the near vanishing result for the K^0 could be due to a near cancellation between the polarizability and the volume effect. Further study at multiple volumes and pion masses is necessary to disentangle the chiral and volume corrections.

B. Charged pion and kaon

We utilize the conventional effective-mass plot in order to display the nonstandard behavior of charged particle correlation functions. In Fig. 3, we display effective-mass plots for the charged pion and charged kaon. In nonvanishing fields, correlators exhibit a clear rise in the effective mass, Eq. (11), with respect to time. The need for a fully relativistic treatment of the two-point function is also evident from the figure as effective-mass shifts are on the order of the rest mass.

Fits to the correlation functions of charged particles have been shown in the effective-mass plots, Fig. 3. We fit the charged particle correlation functions using contributions from two states, as in Eq. (8) Although the amplitudes of the two states, $Z(\mathcal{E})$ and $Z'(\mathcal{E})$, enter the fit function linearly, we have not utilized variable projection due to the increased computational time needed to perform the fits. In zero field, we augmented the correlation function with backwards propagating contributions to the two states. In nonvanishing electric fields, however, we found that backwards propagating charged particles make negligible contributions to the correlation functions. For a 1% effect due to a backwards propagating state, one must go beyond $t = 40$ for the $n = 1$ field strength, and to even larger times in stronger fields. Consequently we ignore backwards propagation in all but the zero-field case. Carrying out time-correlated fits on the bootstrap ensemble, we arrive at an ensemble of rest energies, $\{\boldsymbol{E}_i(\mathcal{E})\}$, for the ground state. At this point, the analysis parallels that of the neutral particles. Fits to the energy function are carried out on the bootstrap ensemble using Eq. (12) producing the mass, polarizability, and quartic coupling. These extracted parameters are then averaged over the bootstrap ensemble. Their uncertainties arise from both fitting and bootstrapping, which we have added in quadrature.

Extracted values of rest energies and fit parameters have been tabulated for the charged pion and kaon in Table II. In performing these fits, we used the fit window $8 \leq t \leq 29$. By comparing fits on adjacent time windows, we can estimate the systematic due to the choice in fit window.

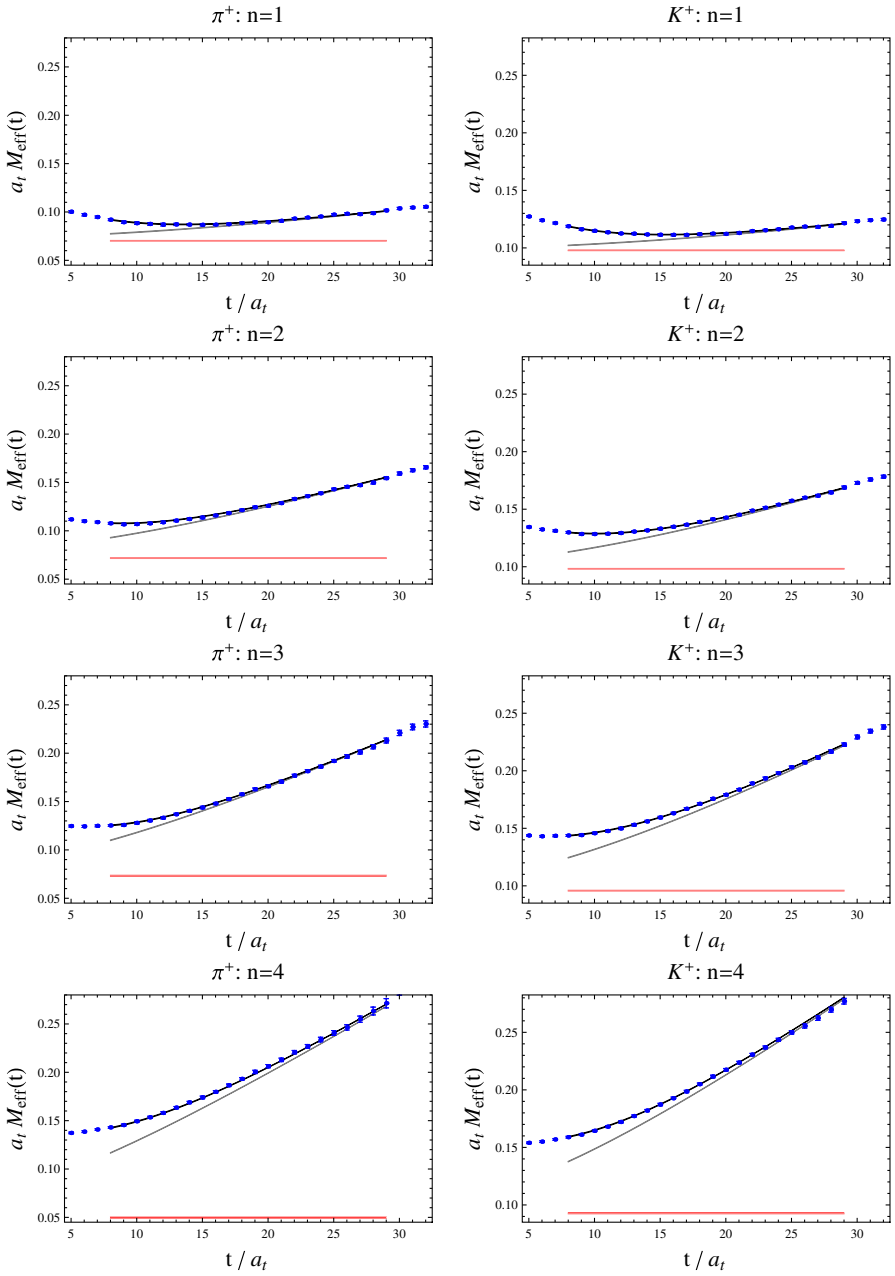

FIG. 3 (color online). Charged pion and kaon effective-mass plots along with two-state fits to the correlation function using Eq. (8). The bands represent the uncertainty from the extracted ground-state rest energy, which is also plotted separately as a flat band. Using the fit parameters $Z(\mathcal{E})$ and $E(\mathcal{E})$, we form the ground-state correlation function which is depicted by the intermediate (gray) bands. Over long times, the effective mass should asymptotically approach these bands. We omit the zero-field plots because they are quite similar to their uncharged counterparts.

We find a large spread in the extracted value of charged particle polarizabilities, and consequently a comparatively large systematic uncertainty due to the fit window. Rest energies are particularly sensitive to the fit window as the field strength increases.

While fits to charged particle correlation functions appear to describe the data well when displayed in terms of the effective mass, a further tool can be used to more clearly present these fits. This tool, moreover, aids in the determination of appropriate fit windows, and we refer to it as the effective energy plot. The effective energy, just like the effective mass, is produced by considering the correlation function at successive times. The relativistic propagator for a charged particle in Eq. (9) depends on the time, the electric field, and rest energy, $D = D(t, E(\mathcal{E}), \mathcal{E})$, albeit through a complicated one-dimensional integral. Given

TABLE II. Summary of fit results for charged meson two-point functions for $8 \leq t \leq 29$. Entries are as in Table I.

	n	$a_t E(\mathcal{E})$	$1-P$		n	$a_t E(\mathcal{E})$	$1-P$
π^+	0	0.0691(4)	0.66	K^+	0	0.0969(3)	0.70
	1	0.0702(6)	0.46		1	0.0979(4)	0.77
	2	0.0718(8)	0.61		2	0.0982(7)	0.78
	3	0.0733(16)	0.93		3	0.0958(10)	0.98
	4	0.0497(129)	0.97		4	0.0927(23)	0.97

π^+	$a_t M$	α_E^{latt}	$\bar{\alpha}_{EEE}^{\text{latt}}$	$1-P$	K^+	$a_t M$	α_E^{latt}	$\bar{\alpha}_{EEE}^{\text{latt}}$	$1-P$
I	0.0692(2)	18(4)(6)	24(10)	0.30	I	0.0971(2)	8(3)(1)	17(5)	0.03
II	0.0692(2)	16(3)(3)	17(10)	0.64	II	0.0969(2)	16(4)(3)	40(9)	0.23

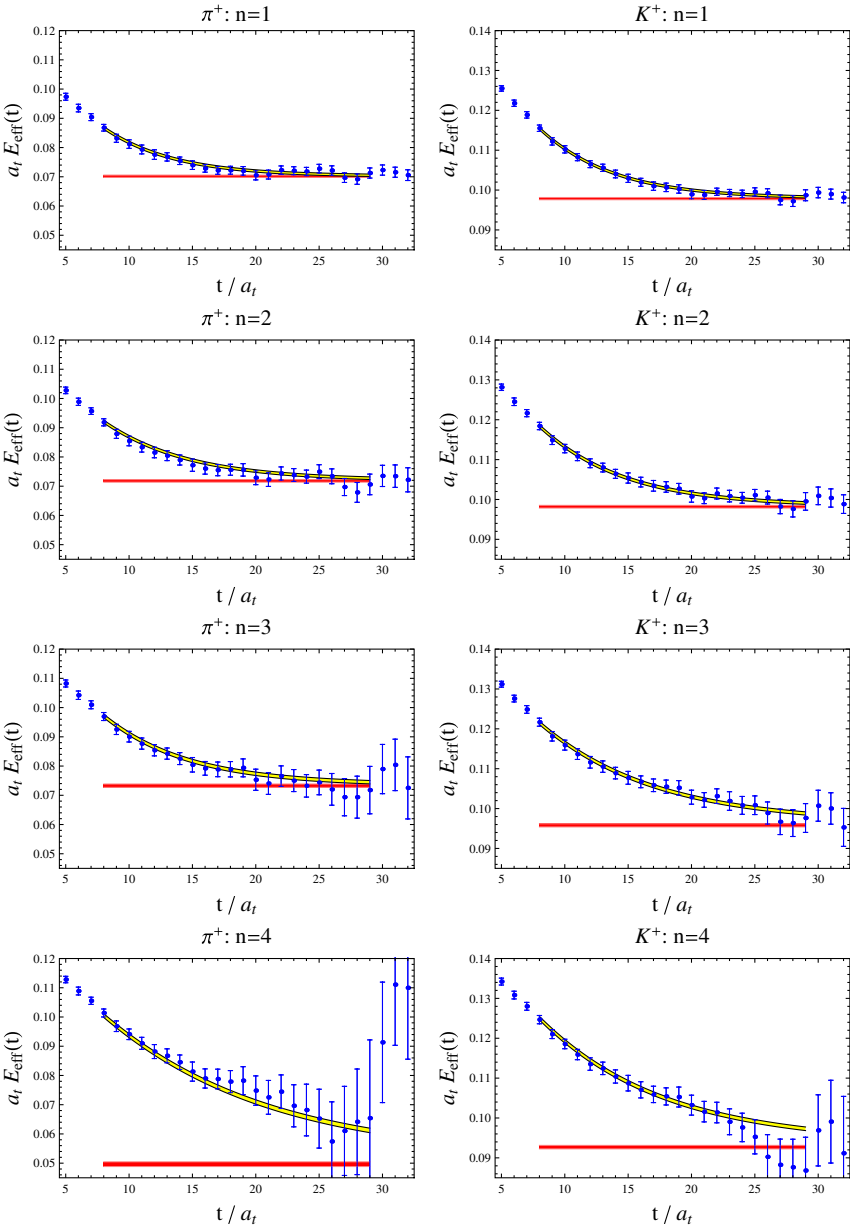

FIG. 4 (color online). Effective energy plots for the charged pion and kaon two-point functions. Fits to the correlation functions are also shown. Values for n correspond to the strength of the quantized electric field $\mathcal{E}$, given in Eq. (3). We have omitted the $n = 0$ plots, as they are just the ordinary effective-mass plots.

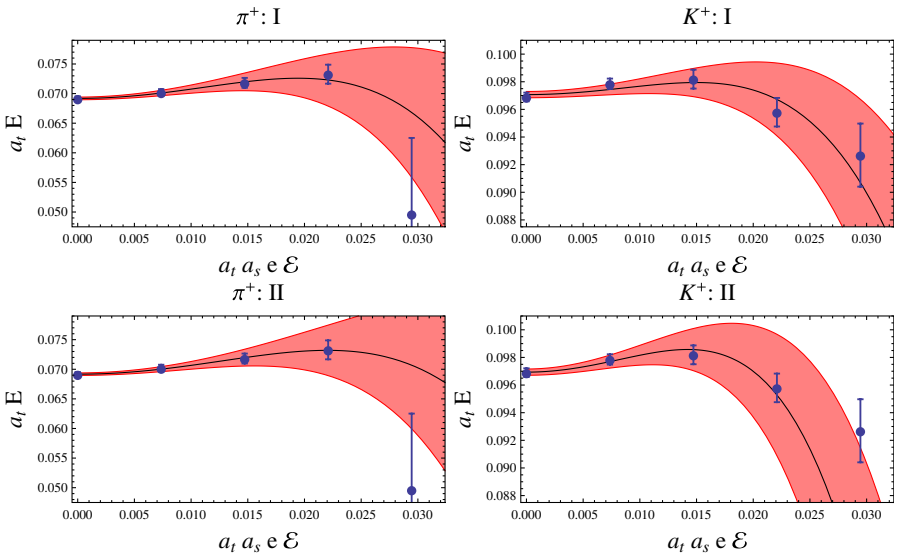

FIG. 5 (color online). Plots of the electric-field dependence of the extracted rest energies for charged mesons.

numerical data for the correlation function, $g(t, \mathcal{E})$, we can successively solve[6] for the effective energy in time by considering the ratio

$$\frac{D(t+1, E_{\text{eff}}, \mathcal{E})}{D(t, E_{\text{eff}}, \mathcal{E})} = \frac{g(t+1, \mathcal{E})}{g(t, \mathcal{E})}, \tag{14}$$

with the value of the electric field, $\mathcal{E}$, as input. This produces the effective energy as a function of time, $E_{\text{eff}}(t)$. Effective energy plots for the charged pion and kaon are shown in Fig. 4. The effective energy should plateau over long times to the rest energy of the charged particle. From the figure, however, we see that contributions from the first excited state linger, and plateaus are not quite reached before the noise grows substantially. Nonetheless, we clearly see behavior reminiscent of the neutral particle effective-mass plots in Fig. 1. This confirms that Eq. (9) properly describes the correlation function of a charged particle in an electric field.

Finally in Fig. 5, we plot the electric-field dependence of the extracted rest energies of the charged pion and kaon. There is striking nonmonotonic behavior which indicates the presence of quartic and perhaps higher-order terms in the field strength. We can make a brief comparison with chiral perturbation theory. The size of the extracted polarizabilities is consistent with naïve expectations, i.e. positive and on the order of 10^{-4} fm^3 in physical units.

[6]Because the effective energy is deduced from the nonlinear relation in Eq. (14), there is no guarantee a solution exists. Ensembles for which no solution can be found at a given time are dropped from the bootstrap. This only affected error bars the $n = 4$ effective energy plot for the π^+, and only for $t \geq 24$, where on average 5 bootstraps were dropped.

V. CONCLUSION

In this work, we have employed constant electric fields on a periodic lattice to investigate meson electric polarizabilities. Sizes of current-day lattices allow the utilization of properly quantized values of the electric field that lead to perturbative shifts in hadron energies. To test our setup, we have shown that the neutral pion (connected part) and kaon polarizabilities can be extracted from lattice QCD by measuring their energies as a function of the applied electric field strength. Furthermore, we have investigated the charged pion and charged kaon polarizabilities, for which simple spectroscopy is of no avail. Using the relativistic charged particle propagator in the presence of an electric field, we fit lattice two-point functions and extract rest energies of charged pions and kaons. Using effective energy plots, we showed that, despite nonstandard behavior for the correlation function, rest energies of charged particles show behavior similar to the effective masses of neutral particles in electric fields. Charged meson polarizabilities were then extracted from the behavior of the rest energy as a function of the electric field. Resulting electric polarizabilities have comparatively large uncertainties due predominantly to two sources. With our current analysis method, the choice of time window gives a larger than expected systematic uncertainty. Global fits, that are correlated in both time and electric field strength, can address such systematic error. Second, higher-order terms in the weak field expansion of charged particle rest energies appear to be very important, prompting future study on larger lattices on which the quantized field strengths are smaller. We hope that further refinements to the fitting procedure, additional data at different volumes and pion masses will remove the largest systematic effects, and ultimately bring lattice QCD in contact with experi-

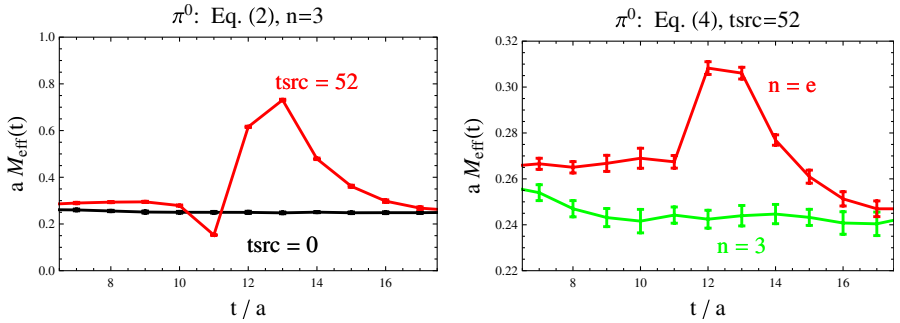

FIG. 6 (color online). Comparison of background field implementation. On the left panel, we fix the field strength and change the source location using Eq. (2) to implement the background field. On the right panel, we fix the source time and change the field strength while using Eq. (4).

mental data for polarizabilities. Ultimately we will also use sea quarks that couple to the background fields.

ACKNOWLEDGMENTS

These calculations were performed using the CHROMA software suite [36] on the computing clusters at Jefferson Laboratory. Time on the clusters was awarded through the USQCD collaboration, and made possible by the SciDAC Initiative. This work is supported in part by Jefferson Science Associates, LLC under U.S. Department of Energy contract No. DE-AC05-06OR-23177 (W. D.). Additional support provided by the U.S. Department of Energy, under Grants No. DE-FG02-04ER-41302 (W. D.), No. DE-FG02-93ER-40762 (B. C. T.), and No. DE-FG02-07ER-41527 (A. W.-L.).

APPENDIX: NONUNIFORM FIELDS

Although we employ quantized field strengths, Eq. (3), with a proper treatment of the boundary flux, Eq. (4), we have additionally explored the effect of nonquantized fields on particle correlators. For this study, we use isotropic $24^3 \times 64$ lattices, the details of which are presented in [21]. We summarize our findings here.

First we consider the naïve implementation of the external field using Eq. (2) and the field value corresponding to $n = 3$ in Eq. (3). In the continuum limit, the spike in the boundary flux contracts to a point and the field becomes uniform. To test the uniformity of the field at finite lattice spacing, we look at the (connected) neutral pion two-point function. If we take the source time at $t_{\rm src} = 0$, then the effective mass exhibits a plateau around $t = 12$, as shown in Fig. 6. On the other hand, if we take the source time at $t_{\rm src} = 52$, then the plateau would set in as the pion wraps around the time boundary. The correlation function shows striking evidence for the spike in the electric field from boundary flux. Notice in plotting we have translated the latter correlation function forward by 12 units in time.

Next we consider the proper implementation of the external field on a torus using Eq. (4). We again consider the (connected) neutral pion two-point function. Fixing the source time at $t_{\rm src} = 52$, we plot in Fig. 6 the resulting effective mass for two values of the field strength, $n = 3$ and $n = e = 2.71828\ldots$. We translate both correlation functions forward by 12 units in time. For $n = e$, the effect of boundary flux has been mitigated (roughly by a factor of 10), but, leads to easily measurable shifts in the particle energy. The quantized value, $n = 3$, exhibits a plateau as the field is uniform across the time boundary.

[1] T. DeGrand and C. DeTar, *Lattice Methods for QCD* (World Scientific, Singapore, 2006).
[2] B. R. Holstein, Comments Nucl. Part. Phys. **19**, 221 (1990).
[3] U. Bürgi, Nucl. Phys. **B479**, 392 (1996).
[4] J. Gasser, M. A. Ivanov, and M. E. Sainio, Nucl. Phys. **B745**, 84 (2006).
[5] Y. M. Antipov *et al.*, Phys. Lett. **121B**, 445 (1983).
[6] J. Ahrens *et al.*, Eur. Phys. J. A **23**, 113 (2005).
[7] P. Abbon *et al.* (COMPASS), Nucl. Instrum. Methods Phys. Res., Sect. A **577**, 455 (2007).
[8] H. R. Fiebig, W. Wilcox, and R. M. Woloshyn, Nucl. Phys. **B324**, 47 (1989).
[9] J. Christensen, W. Wilcox, F. X. Lee, and L.-M. Zhou, Phys. Rev. D **72**, 034503 (2005).
[10] M. Engelhardt (LHPC), Phys. Rev. D **76**, 114502 (2007).
[11] J. Hu, F.-J. Jiang, and B. C. Tiburzi, Phys. Rev. D **77**, 014502 (2008).
[12] B. C. Tiburzi (private communication).
[13] J. S. Schwinger, Phys. Rev. **82**, 664 (1951).
[14] B. C. Tiburzi, Nucl. Phys. **A814**, 74 (2008).
[15] G. 't Hooft, Nucl. Phys. **B153**, 141 (1979).

[16] G. 't Hooft, Commun. Math. Phys. **81**, 267 (1981).
[17] P. van Baal, Commun. Math. Phys. **85**, 529 (1982).
[18] J. Smit and J. C. Vink, Nucl. Phys. **B286**, 485 (1987).
[19] H. R. Rubinstein, S. Solomon, and T. Wittlich, Nucl. Phys. **B457**, 577 (1995).
[20] M. H. Al-Hashimi and U. J. Wiese, Ann. Phys. (N.Y.) **324**, 343 (2009).
[21] W. Detmold, B. C. Tiburzi, and A. Walker-Loud, arXiv:0809.0721.
[22] J. Hu, F.-J. Jiang, and B. C. Tiburzi, Phys. Lett. B **653**, 350 (2007).
[23] B. C. Tiburzi, Phys. Lett. B **674**, 336 (2009).
[24] W. Detmold, B. C. Tiburzi, and A. Walker-Loud, Phys. Rev. D **73**, 114505 (2006).
[25] R. G. Edwards, B. Joo, and H.-W. Lin, Phys. Rev. D **78**, 054501 (2008).
[26] H.-W. Lin *et al.* (Hadron Spectrum), Phys. Rev. D **79**, 034502 (2009).
[27] A. Stathopoulos and K. Orginos, arXiv:0707.0131.
[28] M. Teper, Phys. Lett. B **183**, 345 (1987).
[29] M. Albanese *et al.* (APE), Phys. Lett. B **192**, 163 (1987).
[30] C. Morningstar and M. J. Peardon, Phys. Rev. D **69**, 054501 (2004).
[31] G. T. Fleming, arXiv:hep-lat/0403023.
[32] G. T. Fleming, S. D. Cohen, H.-W. Lin, and V. Pereyra, arXiv:0903.2314.
[33] S. R. Beane *et al.*, arXiv:0903.2990.
[34] J. Bijnens and F. Cornet, Nucl. Phys. **B296**, 557 (1988).
[35] J. F. Donoghue, B. R. Holstein, and Y. C. Lin, Phys. Rev. D **37**, 2423 (1988).
[36] R. G. Edwards and B. Joo (SciDAC), Nucl. Phys. B, Proc. Suppl. **140**, 832 (2005).